Empirical bond-order potential description of thermodynamic properties of crystalline silicon

Lisa J. Porter, Sidney Yip, Masatake Yamaguchi, Hideo Kaburaki, and Meijie Tang

Citation: Journal of Applied Physics **81**, 96 (1997);
View online: https://doi.org/10.1063/1.364102
View Table of Contents: http://aip.scitation.org/toc/jap/81/1
Published by the American Institute of Physics

Empirical bond-order potential description of thermodynamic properties of crystalline silicon

Lisa J. Porter[a] and Sidney Yip
Department of Nuclear Engineering, Massachusetts Institute of Technology, Cambridge, Massachusetts 02139

Masatake Yamaguchi and Hideo Kaburaki
Center for Promotion of Computational Science and Engineering, Japan Atomic Energy Research Institute, Tokai-mura, Naka-gun, Ibaraki 319-11, Japan

Meijie Tang
Lawrence Livermore National Laboratory, P.O. Box 808, L-268, Livermore, California 94550

(Received 5 August 1996; accepted for publication 23 September 1996)

Thermodynamic properties of silicon (diamond cubic phase) are calculated using an empirical many-body potential developed by Tersoff [Phys. Rev. Lett. **56**, 632 (1986)] based on the concept of bond order. It is shown that this model gives predictions in good agreement with experiment for those properties governed by energetics (free energy, entropy, and heat capacity). The thermal expansion coefficient is less well described, which is traced to the fact that the model potential, in its present version, is overly stiff and therefore unable to account properly for the volume dependence of the transverse acoustic modes. Furthermore, sensitivity of the potential to whether each atom remains bonded to only four neighbors indicates that the short-range nature of the potential may necessitate model improvement before it is suitable for studies of thermomechanical properties at elevated temperatures or large deformations. © *1997 American Institute of Physics.* [S0021-8979(97)01701-5]

I. INTRODUCTION

Despite recent advances in simulation methodology and algorithm, computational speed continues to dictate the level of complexity that one can practically study in modeling technologically relevant materials. First-principles quantum mechanical methods generally provide the most reliable and accurate results; however, this approach is still not feasible when large system sizes or long simulation times are involved, such as studies of dislocation mobility in Si (Ref. 1) and transport properties of SiC.[2] Even the calculation of finite temperature properties of perfect crystals poses a significant challenge as can be seen in a recent *ab initio* molecular dynamics calculation of the free energy of Si, where an empirical potential was used for an intermediate step in the calculation.[3]

Empirical interatomic potentials constitute a compromise between accuracy and speed, providing a means of investigating problems that are currently beyond the purely *ab initio* approach. Although an empirical description generally has limited transferability, and its ability to give quantitative results should always be carefully scrutinized, such an approach can be quite useful in exploratory studies (see, for example, Ref. 4). Empirical potentials also may be manipulated to isolate a certain physical effect, thus providing a degree of freedom that is generally not available to the first principles approach. For example, an empirical potential for a binary compound was modified to bring out the importance of size effects in the pressure-induced amorphization of SiC.[5]

There exist many empirical potential models of Si which can be roughly classified into two major categories. The first of these are the potentials that express the cohesive energy as a sum of two- and three-body terms, the most well-known example being the Stillinger–Weber potential.[6] The second category of potentials abandons this approach in favor of a pairwise construction, modified by a bond-order parameter, which explicitly accounts for the variation of bond strength with coordination number.[7–12] Such models are physically appealing because of the simple fact that the chemical bonding between two atoms becomes weaker in local configurations when the number of neighboring atoms increases.[13] The first researcher to implement the concept of bond order in an empirical potential for Si was Tersoff.[7] Several versions of his model now exist; the one with which we are concerned here is the third and most-often-used formulation.[9] The connection between this version and a class of so-called bond-order potentials which can be systematically derived from a tight-binding approximation to the density functional theory of cohesion has been recently discussed.[14]

We have two main objectives:

(1) to delineate the quantitative accuracy of an empirical bond-order potential in describing the thermal properties of Si; and
(2) to probe further the suitability of the Tersoff model for analyzing thermomechanical behavior.

Because finite-temperature properties were not part of the database used in fixing the Tersoff model parameters, they provide a useful test of the potential, besides being important in their own right. From the good agreement between the free energy calculations and experiment we conclude that the model is quite satisfactory as far as energetics is concerned.

[a]Electronic mail: ljporter@mit.edu

 0021-8979/97/81(1)/96/11/$10.00

On the other hand, the thermal expansion coefficient, a manifestation of thermomechanical responses, shows a discrepancy that reveals that the empirical bond-order potential, in the present Tersoff formulation including choice of parameter values, is unable to describe properly some of the angle-dependent forces, especially those involved in the volumetric response of transverse acoustic vibrational modes.

The article is organized as follows. Computational procedure and the potential model are summarized in Sec. II along with the introduction of a scaling factor which relates the temperature of the classical molecular dynamics (MD) simulation to the temperature at which experimental data are obtained. Energy calculations are presented in Sec. III in terms of internal energy, free energy, entropy, and heat capacity; the MD results are compared with the harmonic approximation, experimental data, and results from both *ab initio* and Stillinger–Weber calculations. The study of thermal expansion is discussed in Sec. IV where we examine the discrepancy between the Tersoff model and experiment through the Grüneisen parameter. In Sec. V we discuss another aspect of the Tersoff model, the interaction range cutoff, which would require attention whenever the potential is used at high temperatures. In the concluding remarks, Sec. VI, we suggest future directions for continuing the development of an empirical bond-order potential that was initiated by Tersoff.

II. POTENTIAL MODEL AND METHODOLOGY

A. Tersoff model

The Tersoff potential model that we adopt in this work has been described in detail previously;[15] relative to the original potential description,[9] the interaction range cutoff is now treated as a variable parameter which scales with one-third power of the volume.

B. Temperature scaling

All the MD simulations were carried out using a periodic cubic cell of 216 atoms with an integration time step of 0.26 fs. Size effects were tested using a cell of 512 atoms, and no significant differences in any of the properties were found. The zero-pressure lattice parameter at each specified temperature was determined by using the Parrinello–Rahman method,[16] allowing 20 000 time steps for equilibration and the next 5000–10 000 time steps for time averaging. Values of the lattice parameters so obtained were checked by performing constant-volume simulations using these values, which yielded essentially zero average pressure (1 kBar or less, typically less than 0.1 kBar) and energies that were equivalent to the constant-pressure values within statistical error.

Because MD simulations obey the rules of classical statistical mechanics, quantum corrections are necessary when comparing with experimental results, particularly at low temperatures. We have adopted the procedure of Wang, Chan, and Ho,[17] in which the simulation temperature T_{MD} is related to a scaled temperature T_{real} by requiring that the internal energy of the classical simulation system at T_{MD} be equal to that of the corresponding quantum system at T_{real}. That is,

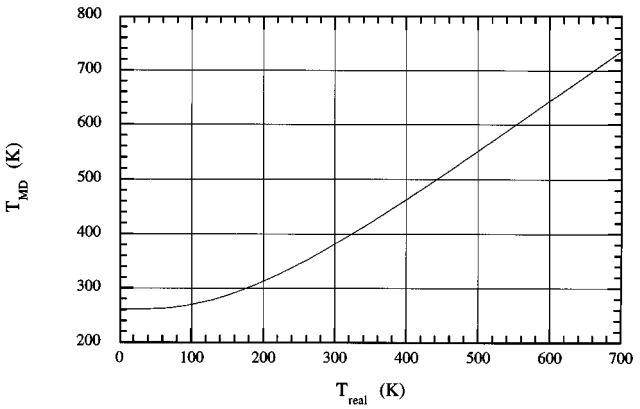

FIG. 1. Temperature scaling for silicon. $T_{\mathrm{MD}}=263.85-0.165\,68T_{\mathrm{real}}+0.002\,506\,1T_{\mathrm{real}}^2-(2.2261\times10^{-6})\,T_{\mathrm{real}}^3-(5.0875\times10^{-11})\,T_{\mathrm{real}}^4+(8.1956\times10^{-13})T_{\mathrm{real}}^5$ (T_{MD} and T_{real} in K).

$$3(N-1)k_BT_{\mathrm{MD}}=\frac{1}{2}\sum_i \hbar\omega_i+\sum_i \frac{\hbar\omega_i}{\left[\exp\left(\frac{\hbar\omega_i}{k_BT_{\mathrm{real}}}\right)-1\right]}, \tag{2.1}$$

where ω_i is the ith normal mode frequency, the sum runs from $i=1$ to $3(N-1)$, and N is the number of particles in our system. The factor $(N-1)$ appearing on the left-hand side accounts for the fact that the center of mass of the simulation cell is held fixed.

The normal modes are obtained by diagonalizing the force-constant matrix,

$$D_{i\alpha j\beta}=\frac{\partial^2 U}{\partial r_{i\alpha}\partial r_{j\beta}}, \tag{2.2}$$

where U is the interatomic potential, indices i and j denote atom number, and α and β denote Cartesian components. The force-constant matrix for the Tersoff model has been derived analytically; to our knowledge the results (given in the Appendix) have not been reported previously.

The scaling relation between T_{MD} and T_{real} is shown in Fig. 1, where the phonon frequencies are those determined at $T_{\mathrm{MD}}=0$ K. Note that when $T_{\mathrm{real}}=0$ K, $T_{\mathrm{MD}}=261.9$ K, which we regard as the zero-point temperature of our model system (corresponding to a zero-point energy of 0.0674 eV/atom). The relation (2.1) follows from the assumption that the internal energies of both the MD system and the real system behave harmonically, at least at low temperatures, where the scaling is important. We have found that in fact the behavior of the internal energy determined by MD simulation is quite harmonic over a wide temperature range (see the following section). As a simple check, we have recomputed the force-constant matrix using the lattice parameter determined at $T_{\mathrm{MD}}=261.9$ K and have found that the phonon frequencies obtained at this lattice parameter yield a scaling relation essentially identical to Fig. 1 and give a zero-point temperature of 260.5 K. Throughout this work, temperature will be taken to mean T_{real}; thus, when an MD result is presented at a certain temperature, the simulation temperature T_{MD} has been scaled according to Eq. (2.1).

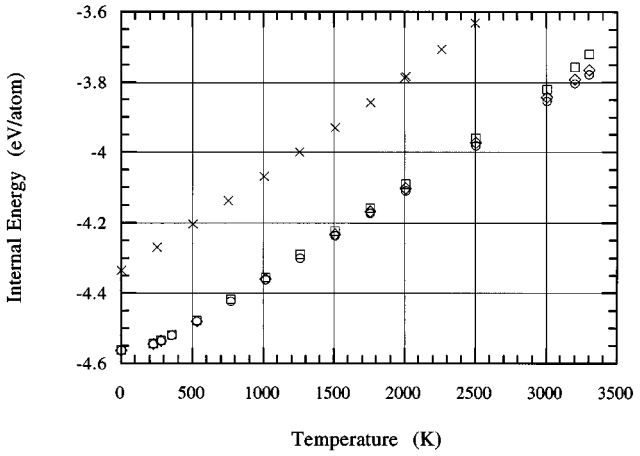

FIG. 2. Variation of internal energy with temperature for the HA (circles), QHA (diamonds), MD (squares), and Stillinger–Weber values (see Ref. 18) (crosses).

C. Harmonic and quasiharmonic calculations

In the harmonic approximation one has standard expressions for the internal energy, the Helmholtz free energy, and the heat capacity at constant volume,

$$E = U_0 + \frac{1}{2}\sum_i \hbar\omega_i + \sum_i \frac{\hbar\omega_i}{[\exp(\hbar\omega_i/k_BT)-1]}, \quad (2.3)$$

$$F = U_0 + \frac{1}{2}\sum_i \hbar\omega_i + k_BT\sum_i \ln\left[1-\exp\left(-\frac{\hbar\omega_i}{k_BT}\right)\right], \quad (2.4)$$

$$C_V = k_B\sum_i \frac{(\hbar\omega_i/k_BT)^2\exp(\hbar\omega_i/k_BT)}{[\exp(\hbar\omega_i/k_BT)-1]^2}, \quad (2.5)$$

where U_0 is the static lattice energy. Results presented which are denoted as HA are obtained using the force-constant matrix evaluated for a static lattice, $T_{\mathrm{MD}}=0$ K. We also present results denoted as quasiharmonic or QHA; for these, the force-constant matrix and the static energy are evaluated at the zero-pressure lattice parameter determined for that particular temperature.

III. RESULTS: INTERNAL ENERGY, FREE ENERGY, ENTROPY, HEAT CAPACITY

Fig. 2 shows the temperature variation of the internal energies obtained by MD simulation, HA, and QHA. (No *ab initio* results are available for comparison.) Also shown in Fig. 2 are MD results for the potential model of Stillinger and Weber.[18] Anharmonic effects are seen to be quite small; even at $T=3300$ K, the HA and QHA are within 1.6% and 1.2% of the MD result, respectively. That the perfect crystal is still stable at such temperature (experimental melting point of silicon is 1683 K) indicates that the melting point corresponding to the Tersoff model is considerably greater than the experimental value (see also Refs. 19–21). Also, the absence of defects of any kind allows the crystal to be superheated to its limit of metastability.

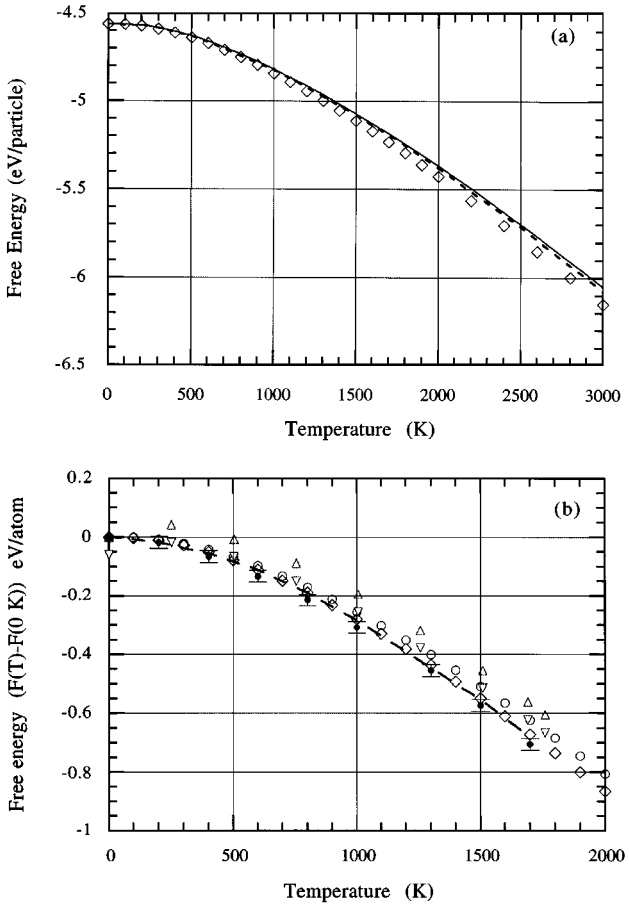

FIG. 3. Variation of free energy with temperature: (a) for the HA (solid line), QHA (dashed line), and MD (diamonds); and (b) for the HA (circles), MD (diamonds), *ab initio* from Fig. 2 of Ref. 3 (filled circles), Stillinger–Weber, classical approximation (see Ref. 18) (triangles), Stillinger–Weber corrected for zero-point energy (upside-down triangles), and experimental data from Fig. 2 of Ref. 3 (dashed line).

To obtain the Gibbs free energy G one can directly integrate the thermodynamic relation

$$\frac{d}{dT}\left(\frac{G}{T}\right) = -\frac{H}{T^2}, \quad (3.1)$$

where H is the enthalpy. At zero pressure $H=E$ and $G=F$. The integration constant can be fixed in various ways;[18,21–23] it turns out that the results are not very sensitive to whichever method is used. Over the temperature range under consideration, internal energies at 15 temperatures were calculated; Eq. (3.1) was then integrated using a sixth-order polynomial fit of $H(T)$. Figure 3(a) compares the HA, QHA, and MD values of the free energy and shows that the anharmonic effects are quite small, consistent with our findings for the internal energy. In Fig. 3(b) we see that, in comparison with experiment, the Tersoff potential does almost as well as the *ab initio* calculation.[3] The Stillinger–Weber results[18] differ significantly from the *ab initio* results, but the agreement is greatly improved if one makes a simple correction to account for the fact that the classical approximation was used, by subtracting the *ab initio* value for the zero-point energy of 0.06 eV/atom. [Ungar and co-workers[21] have obtained the

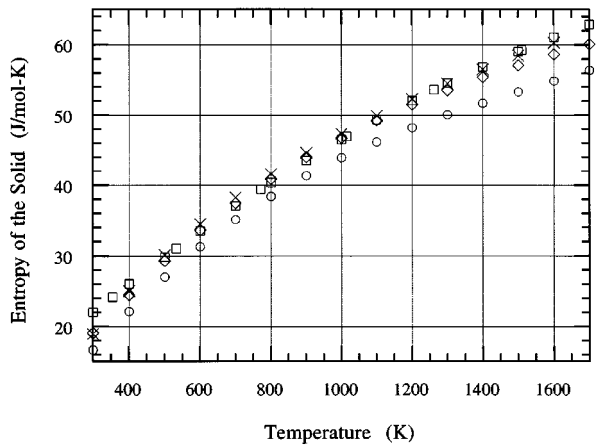

FIG. 4. Variation of entropy with temperature for the HA (circles), MD method 1-c1 (diamonds), *ab initio* (squares), obtained from third-order polynomial fit of $G(T)$ from Fig. 2 of Ref. 3, and experiment (see Refs. 24 and 25) (crosses).

free energy of bulk Si in the classical regime ($T \geqslant 500$ K) using Monte Carlo (MC) simulation and the Tersoff potential. Our results are consistent with the values displayed in Fig. 1 of Ref. 21.]

Entropies are obtained from the thermodynamic relation

$$S = -\frac{dG}{dT}. \tag{3.2}$$

Figure 4 shows that the Tersoff results are in generally good agreement with *ab initio* calculations[3] and experiment.[24,25] Because only the vibrational entropy is given by MD simulation, one can infer that the configurational contribution is essentially negligible. In Fig. 4 one sees again that the anharmonic effects are rather small: The underestimate incurred in the harmonic approximation is no more than 12%.

Heat capacity is calculated in a standard way, fitting the temperature variations of E obtained by simulations at constant volume or constant (zero) pressure. Figure 5 shows the comparison with experiment[26] and with the harmonic approximation. It is clear that both the HA and MD values are in very good agreement with experiment.

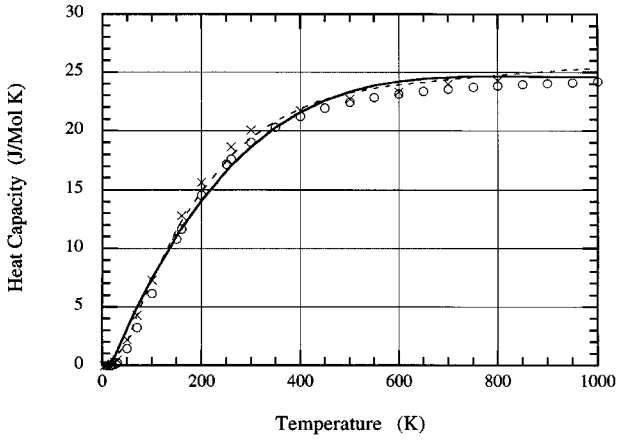

FIG. 5. Variation of heat capacity with temperature for the HA (circles), MD C_v (solid line), MD C_p (dashed line), and experiment (see Ref. 26) (crosses).

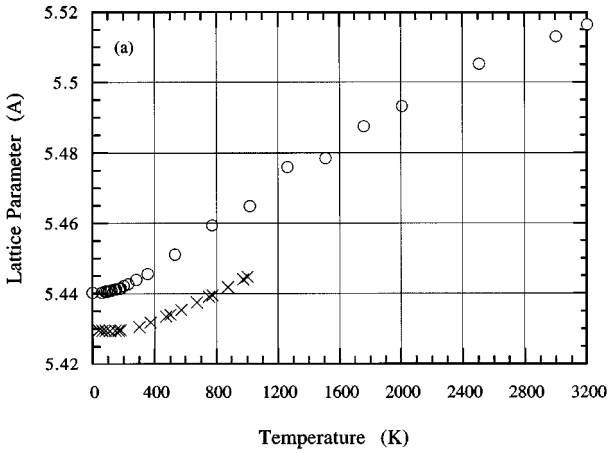

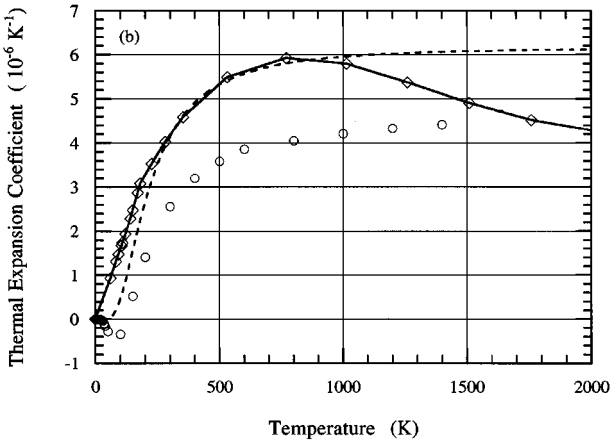

FIG. 6. Temperature dependence of (a) lattice parameter for Tersoff (circles) and experiment (see Ref. 24) (crosses), and (b) thermal expansion coefficient for Tersoff, using MD (solid line with diamonds), using the harmonic approximation (dashed line), and experiment (see Ref. 24) (open circles).

IV. THERMAL EXPANSION COEFFICIENT

We have calculated the thermal expansion coefficient α in two ways. The first approach was to obtain the lattice parameter $a(T)$ at various temperatures using the Parrinello–Rahman technique in MD simulation. Figure 6(a) shows the results which are generally within 0.4% of the experimental values. To obtain α which is defined by

$$\alpha = \frac{1}{a}\frac{da}{dT}, \tag{4.1}$$

we fit the simulation data in Fig. 6(a) with a fifth-order polynomial separately in the low- and high-temperature regions, the crossover being about 180 K. The comparison of the thermal expansion coefficient determined in this manner with experiment is shown in Fig. 6(b). In the very low-temperature region, $T < 200$ K, our results are quite uncertain because the scaling relation is necessarily flat (see Fig. 1).

Figure 6(b) also shows the results obtained using the harmonic approximation for α,[27]

$$\alpha(T)=\frac{1}{3B(T)}\sum_{\mathbf{k},n}\gamma_n(\mathbf{k})C_{vn}(\mathbf{k},T), \tag{4.2}$$

where $B(T)$ is the isothermal bulk modulus,

$$\gamma_n(\mathbf{k})=-\frac{d\{\ln[\omega_n(\mathbf{k},V)]\}}{d(\ln V)} \tag{4.3}$$

is the Grüneisen parameter, and $C_{vn}(\mathbf{k},T)$ is the mode contribution to the specific heat,

$$C_v(T)=\sum_{\mathbf{k},n}C_{vn}(\mathbf{k},T)$$

$$=\sum_{\mathbf{k},n}\frac{\hbar\omega_n(\mathbf{k},V)}{V}\frac{d}{dT}\left[\exp\left(\frac{\hbar\omega_n(\mathbf{k},V)}{k_BT}\right)-1\right]^{-1}. \tag{4.4}$$

As can be seen, while the harmonic approximation is superior to the MD method at low temperatures, both methods yield values which are much larger than the experimental values. Moreover, above 800 K, the MD results show a decrease with temperature, a result which is explained in Sec. 5.

Equation (4.2) indicates a way of analyzing further the behavior of α. Since we have already seen that the heat capacity is well described by the Tersoff potential (cf. Fig. 5), it follows that the deviation from experiment in Fig. 6(b) must be caused by the Grüneisen parameter. We have evaluated Eq. (4.3) by using a linear fit to the phonon frequencies calculated at three system volumes, V_0 and $(1\pm0.03)V_0$, where V_0 is the equilibrium volume for $T_{\mathrm{MD}}=0$ K. A direct comparison of $\gamma_n(k)$ along various high-symmetry directions in the reciprocal lattice with experiment[28] and with *ab initio* calculations[29] is shown in Fig. 7(a). It should be noted that, in contrast with the Tersoff potential, the *ab initio* results for the thermal expansion coefficient are in almost perfect agreement with experiment up to 800 K.[29]

It is clear from Fig. 7(a) that for the transverse acoustic modes the Grüneisen parameter given by the Tersoff potential does not extend to large enough negative values, thus leading to an overestimate of α. Indeed, it is widely accepted that the anomalous negative thermal expansion of silicon at low temperatures is due to the negative γ_n for the TA phonons.[29,30] Furthermore, the Tersoff potential somewhat overpredicts γ_n for the optic modes, which also contributes to the deviation from experiment. In Table I we compare the Tersoff values with other available results for γ_n; besides *ab initio*[29] and experiment,[28] these include a tight-binding calculation[17] and the Stillinger–Weber potential.[17] We note that the Stillinger–Weber result for γ_n at TA(X) is even worse than that for the Tersoff potential. It seems that this parameter could serve as a stringent test for any empirical potential function for Si.

From the mode-specific γ_n one obtains an overall Grüneisen parameter $\gamma(T)$ through the weighted average

$$\gamma(T)=\frac{1}{C_v(T)}\sum_{\mathbf{k},n}\gamma_n(\mathbf{k})C_{vn}(\mathbf{k},T)=3B(T)\frac{\alpha(T)}{C_v(T)}. \tag{4.5}$$

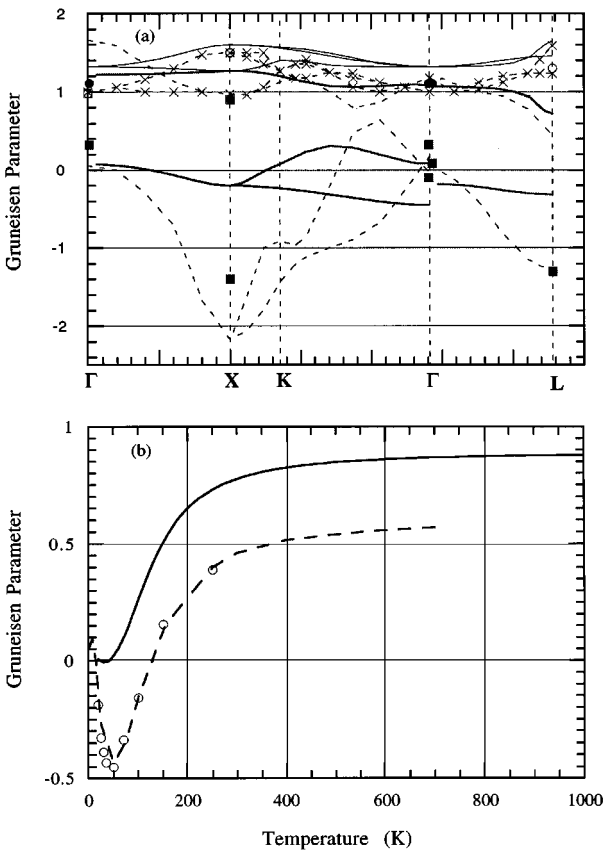

FIG. 7. Grüneisen parameters. (a) Experimental data (see Ref. 28) are given by solid squares (TA modes), solid circles (LA mode), open circles (TO mode), and open squares (LO mode). Thick solid lines correspond to acoustic modes as predicted by Tersoff, thin solid lines correspond to optical modes as predicted by Tersoff, dashed lines correspond to acoustic modes as given by *ab initio*, (see Ref. 29) and dashed lines with crosses correspond to optical modes as given by *ab initio*. (b) Overall Grüneisen parameter for Tersoff (solid line), *ab initio* (see Ref. 29) (dashed line), and experiment (taken from Ref. 29) (circles).

In Fig. 7(b) this quantity is shown along with *ab initio* and experimental values. It is seen that the Tersoff potential overestimates considerably $\gamma(T)$ at all temperatures. From the foregoing discussion, it is clear that this behavior is caused primarily by a less than satisfactory description of the volume dependence of the TA modes. One can further understand the inadequacy by using a simple model for the TA modes[30] in which the restoring force on the atoms is represented by two contributions: a central-force component which is always negative, and an angular-force component which is always positive. The former is inversely proportional to the square of the frequency corresponding to the

TABLE I. Grüneisen parameters.

	Experiment	*ab initio*	Tight binding	Tersoff	Stillinger–Weber
$\gamma_{\mathrm{LTO}}(\Gamma)$	0.98	1.00	0.98	1.32	0.80
$\gamma_{\mathrm{TA}}(X)$	−1.40	−2.18	−1.12	−0.20	−0.04
$\gamma_{\mathrm{TO}}(X)$	1.50	1.50	1.37	1.60	0.89
$\gamma_{\mathrm{LOA}}(X)$	0.90	0.97	1.02	1.27	0.83

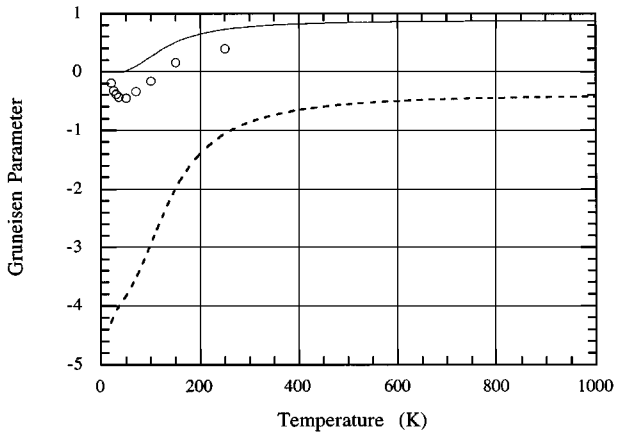

FIG. 8. Grüneisen parameter as a function of temperature for T3 (solid line), T2 (dashed line), and experiment (circles).

equilibrium volume [see Eq. (8) of Ref. 30], whereas the latter arises from the directional covalent bonds which stabilize the diamond structure. A model that either overestimates the TA mode frequencies or overemphasizes the importance of the angular force will therefore overestimate the thermal expansion coefficient. It turns out that the Tersoff model does both.

Besides contributing to the value of $\alpha(T)$ through the Grüneisen parameter, the strength of the bond-angle restoring forces also governs the magnitude of the shear elastic constant C_{44}. After an earlier version (which we call T2 in the present discussion) of the Tersoff model was proposed,[8] it was found that the bond-angle restoring forces were too weak, resulting in a prediction of C_{44} almost an order of magnitude smaller than the experimental value of 0.8 Mbar. The present version of the Tersoff model (called T3) gives a considerably better value of $C_{44}=0.7$ Mbar. In Fig. 8 we see that the $\gamma(T)$ obtained using T2 is clearly much too negative, resulting in a negative α for all T up to 2000 K, in accord with results quoted in Ref. 8. Given the simple model of Ref. 30, these results are completely consistent: The weak angular restoring forces yield both a C_{44} and an α which are much too small. Moreover, the values of the TA mode frequencies for T2 are too low, causing a further underestimation of $\gamma(T)$ through the central-force contribution.

An instructive comparison of T2 and T3 can be made through the bond-order parameter b_{ij} which is a measure of the bond strength between atoms i and j in the presence of other atoms in the immediate vicinity. This parameter has the functional form

$$b_{ij}=\frac{1}{(1+\beta^n\zeta_{ij}^n)^{1/2n}}, \tag{4.6a}$$

where

$$\zeta_{ij}=\sum_{k\neq i,j} f_c(r_{ik})g(\theta_{ijk}). \tag{4.6b}$$

The quantities β and n are fitted parameters which are not pertinent to our discussion. The function $f_c(r_{ik})$ determines whether an atom k should be considered as being in the neighborhood of the bond, and the function $g(\theta)$ is given by

$$g(\theta)=1+\frac{c^2}{d^2}-\frac{c^2}{[d^2+(h-\cos\theta)^2]}, \tag{4.7}$$

where the constants c, d, and h have specified values which differ between T2 and T3 as shown in Table II. It is this angular function that determines how well the potential model describes the directional bonding. In Figs. 9(a) and 9(b) we show $g(\theta)$ for T2 and T3, respectively. Notice the large difference between the two models in both magnitude and qualitative angular variation.

TABLE II. Comparison of parameters for T2 and T3.

Parameter	$T2$	$T3$
c	4.8381	1.0039×10^5
d	2.0417	16.218
h	0.00	−0.59826
g (θ=0°)	2.0864	3.6854×10^5

On the basis of a comparison of $g(\theta)$ for T3 and a corresponding angular function which appears in the systematic formulation of a class of bond-order potentials (BOP) based on the tight-binding approximation,[14] it has been suggested that the Tersoff model has similar properties to the lowest order term in the expansion. More specifically, $g(\theta)$ for T3 is

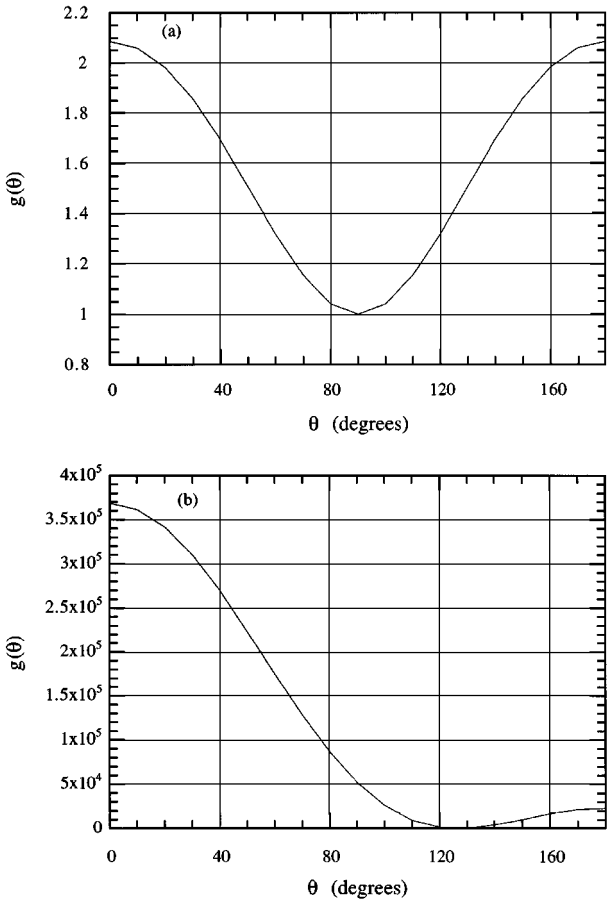

FIG. 9. $g(\theta)$ for (a) T2 and (b) T3.

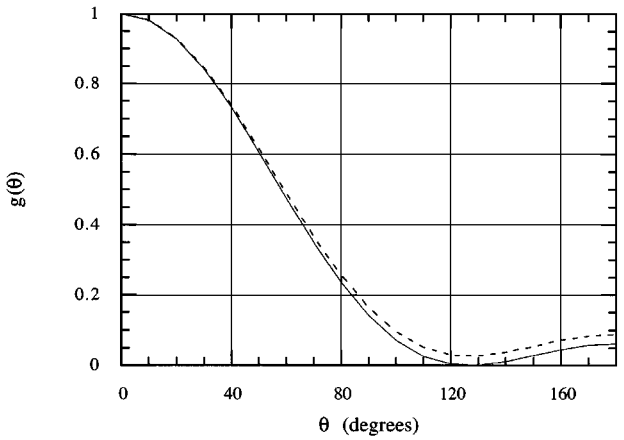

FIG. 10. $g(\theta)$, normalized by $g(0°)$ for T3 (solid line) and T3 with $c=c/100$ (dashed line). The value of $g(0°)$ for T3 is 10^4 times larger than that for T3 with $c=c/100$.

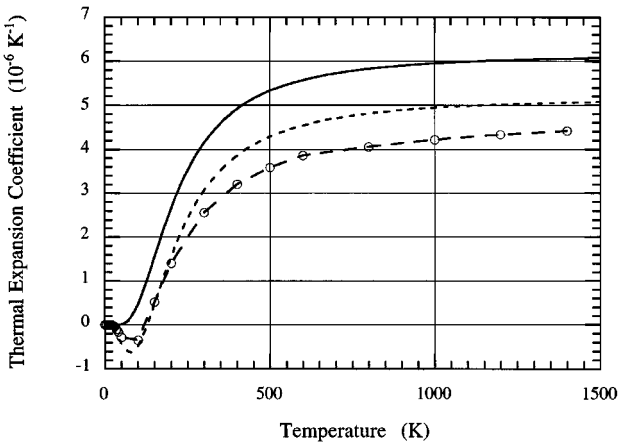

FIG. 12. Thermal expansion coefficient as a function of temperature for T3 (solid line), T2 with $h=-0.60$ (dashed line), and experiment (dashed with circles).

essentially identical to that of the equivalent BOP expression for the σ bond, once $g(\theta)$ is normalized by its value at $g(0°)$. However, we wish to emphasize here that both the functional form and the magnitude of $g(\theta)$ play an important role in describing correctly directional bonding.

To illustrate our point, the following numerical modifications are instructive. If the value of c were reduced by two orders of magnitude in T3, the resulting shape of $g(\theta)$ would be essentially unchanged (see Fig. 10), whereas its magnitude is greatly reduced [$g_0 \equiv g(\theta=0)$ is reduced by a factor of 10^4]. As a result of this modification, the calculated C_{44} becomes smaller than the experimental value by about two orders of magnitude, and correspondingly $\alpha(T)$ becomes far too negative for all temperatures. If a modification were made in T2, such as changing h from 0.0 to -0.60, one would then obtain the $g(\theta)$ shown in its normalized form in Fig. 11, along with the normalized $g(\theta)$ for T3, and it should be noted that the resulting g_0 is smaller than that for T3 by five orders of magnitude. In this case, one finds C_{44} to be 0.51 Mbar, a fivefold increase over the value for T2, and a greatly improved $\alpha(T)$ (see Fig. 12). As a third modification, we consider changing the shape of $g(\theta)$ in T3 while maintaining its large magnitude. This can be accomplished by simply setting $h=0$, and the effect is shown in Fig. 13. For this case C_{44} becomes about an order of magnitude less than the experimental value, and about 15% less than that of T2, and $\alpha(T)$ is negative for T up to 2000 K, although it is much greater than that of T2, as seen in Fig. 14. It is interesting to note that this modification gives a C_{44} that is smaller than that of T2, while the value of $\alpha(T)$ is significantly greater. This is a situation where the central-force contribution plays an important role. (The frequencies of the TA modes in T2 are less than those of this case, yielding a greater negative contribution to γ from the central force.) Taking these examples altogether, we infer that it is a combination of the magnitude and shape of $g(\theta)$ which controls the description of directional bonding in the Tersoff model.

V. MODEL LIMITATIONS AT HIGH TEMPERATURES

While the foregoing analysis has shown that prediction of the thermal expansion coefficient depends on the proper description of the volume dependence of the TA mode fre-

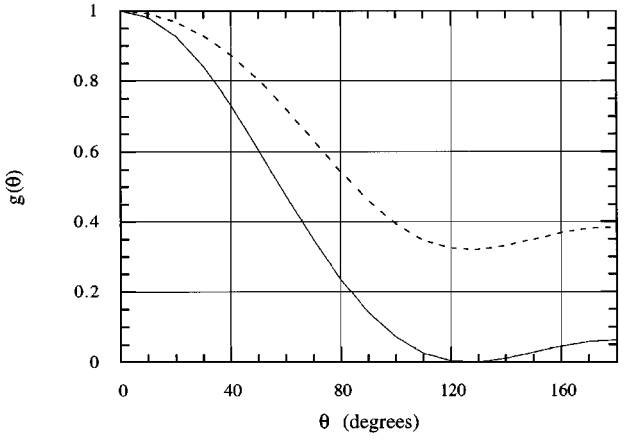

FIG. 11. $g(\theta)$, normalized by $g(0°)$ for T3 (solid line) and T2 with $h=-0.60$ (dashed line). The value of $g(0°)$ for T3 is $\approx 10^5$ times larger than that for T2 with $h=-0.60$.

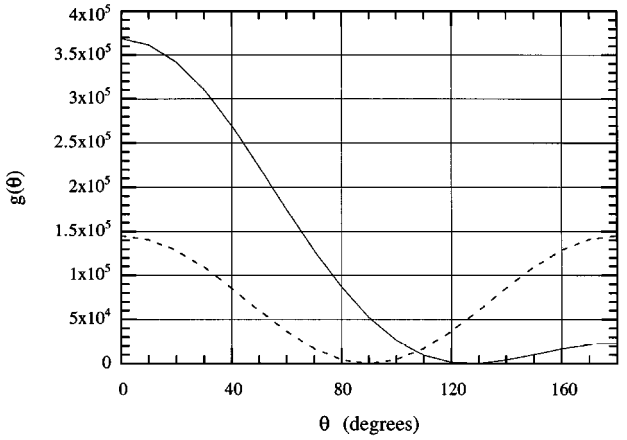

FIG. 13. $g(\theta)$ for T3 (solid line) and T3 with $h=0.0$ (dashed line).

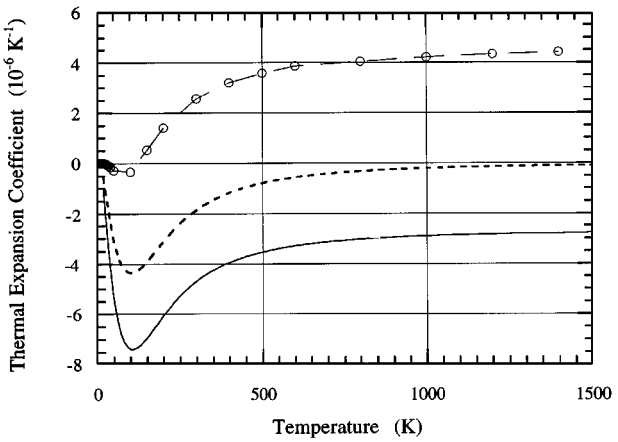

FIG. 14. Thermal expansion coefficient as a function of temperature for T2 (solid line), T3 with $h=0.0$ (dashed line), and experiment (dashed with circles).

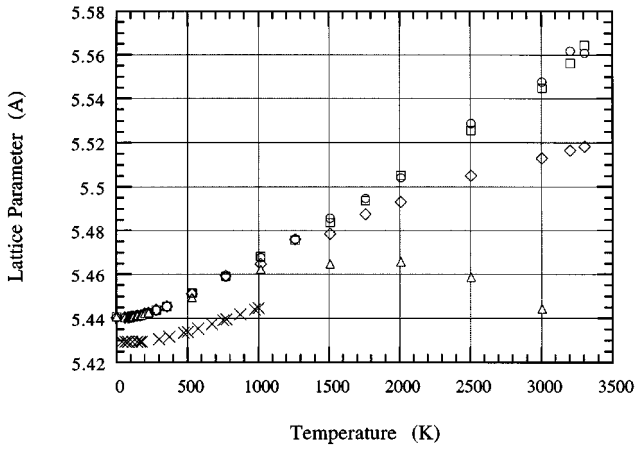

FIG. 15. Variation of lattice parameter with temperature for case 1 ($R/S=2.6/2.8$ Å) (triangles), case 2 ($R/S=2.7/3.0$ Å) (diamonds), case 3 ($R/S=2.8/3.2$ Å) (circles), case 4 (count only the four neighbors of the static lattice) (squares), and experimental data (see Ref. 24) (crosses).

quencies, the behavior of α above 800 K as predicted by MD is further exacerbated by the sensitivity of the potential model to the local coordination number. In the Tersoff model the cohesive energy has contributions only from nearest-neighbor interactions and this restriction is enforced through the introduction of interaction range cutoffs. Two parameters are specified: an inner separation distance R beyond which the two atoms cannot interact with full strength, and an outer separation distance S beyond which two atoms do not interact. A cutoff function appears in the potential such that from R to S it varies smoothly from unity to zero. Unlike the other nine parameters of the model, the values of R and S were not optimized in developing the potential; they were simply chosen to lie between the first and second nearest neighbors on a static lattice.

At sufficiently elevated temperatures, thermal vibrations of the atoms make it possible for the second-nearest neighbors (defined according to the static lattice) to move within a distance S of an atom, causing an increase in its coordination number. The result is a large increase in the energy of the system. The lattice will then expand to try to keep the second-nearest neighbors from interacting. It is also possible for a nearest neighbor to move out of the interaction range, leaving an atom with only three nearest neighbors. This too results in an energy increase, followed by a lattice contraction in response. In either case, lattice expansion or contraction is governed by the strong preference for a purely tetrahedral environment that is intrinsic to the Tersoff model.

The sensitivity of the Tersoff model to range cutoff effects is best illustrated with numerical results on physical properties obtained using different sets of R and S (R/S) values. We consider four cases:

(1) relatively short cutoffs distances, $R/S=2.6/2.8$ Å;
(2) intermediate distances, $R/S=2.7/3.0$ Å;
(3) relatively long distances, $R/S=2.8/3.2$ Å; and
(4) in lieu of cutoffs, every atom interacts with its four nearest neighbors (based on the static lattice) and only these four, no matter what the separation distances.

The temperature variations of the calculated lattice parameter and thermal expansion coefficient are shown in Figs. 15 and 16, respectively, along with the experimental data. From Fig. 15 it is clear that for case (1) the cutoffs are too small: The crystal must actually contract to keep nearest neighbors within the interaction zone above 2000 K. Clearly, this is unphysical (the crystal has not melted). Indeed, the fact that cases (3) and (4) yield similar results indicates that even case (2) exhibits some effect of the nearest neighbors moving out of the interaction zone (see also Ref. 21). In fact, this explains why the thermal expansion coefficient decreases with temperature above 800 K for case (2). In Fig. 16 we see that the variation of α with temperature is better predicted by cases (3) and (4), suggesting that the Tersoff model investigated here is best suited to atomic configurations where fourfold coordination is maintained.

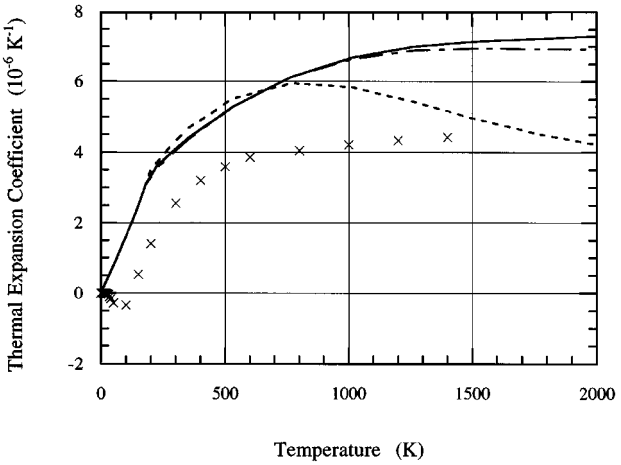

FIG. 16. Variation of thermal expansion coefficient with temperature for case 2 ($R/S=2.7/3.0$ Å) (dashed line), case 3 ($R/S=2.8/3.2$ Å) (solid line), case 4 (count only the four neighbors of the static lattice) (long and short dashed line), and experiment (see Ref. 24) (crosses).

VI. DISCUSSIONS

We have shown that for the purpose of predicting thermodynamic properties of diamond cubic silicon which involve only energetics of the lattice, MD simulation using the Tersoff potential gives results at the caliber of *ab initio* calculations, without the computational expense. In fact, even the simple harmonic approximation is quite acceptable, thus eliminating the need for simulations. On the other hand, *ab initio* models are far better at predicting the thermal expansion coefficient, because the Tersoff potential does not give a good description of the volume dependence of the TA mode frequencies. This is due in large part to the fact that the potential has been designed to yield large bond-angle restoring forces, in order to give a reasonable value of c_{44}. In addition, the potential overpredicts the magnitudes of the TA phonon frequencies.

Further scrutiny of the Tersoff model has led to two additional observations. The first concerns the connection between the Tersoff model,[9] developed heuristically and empirically, and the systematic and deductive formulation of the bond-order potentials (BOP).[14] Although the angular function $g(\theta)$ for T3 is similar in shape with that of the σ bonds in BOP,[14] it does not follow, without more explicit calculations and comparisons, that these two descriptions will give similar results for physical properties. Work along this direction will be of interest. The second observation is that further optimization of the Tersoff model, if desired, should take into account both C_{44} and $\alpha(T)$. Indeed, in most developments of empirical potential models, the thermal expansion coefficient is usually not considered in the database for fitting parameters, and yet it is a fundamental thermomechanical property.

Interestingly, the application of the Tersoff potential[31] to the binary compound SiC has resulted in the prediction of the thermal expansion coefficient in quantitative agreement with experiment (within 15%), once the cutoff effects are accounted for at high temperatures.[2] This can be explained by noting that directional bonding in SiC is stronger than in Si, which is why the thermal expansion coefficient of SiC is always positive. Thus, the Tersoff potential is expected to be adequate for covalent systems where the directional bonding is strong, such as SiC and carbon. (Indeed, good agreement with experiment is also found in the case of diamond.[32]) We anticipate that for germanium, which also has a negative thermal expansion at low temperatures, one would encounter the same difficulty as with Si in applying the Tersoff model.

The issue of sensitivity to range cutoff in the Tersoff potential which we have raised but not fully addressed, needs further attention in applications involving elevated temperatures and large mechanical deformations. Similar concerns also exist in using the model to study disordered structures (see also Refs. 19–21). Because empirical potentials for silicon will continue to play an important role for some time in allowing large-scale simulations beyond the range of electronic-structure methods to be performed, better understanding of the applicability of these potentials, of which the Tersoff model is a significant member, is still needed.

ACKNOWLEDGMENTS

This work has been supported by the AFOSR through Grant No. 91-0285 and the Japan Atomic Energy Research Institute. We are grateful to M. Fearn, J. Broughton, J. Chelikowsky, and R. Dorris for helpful correspondence.

APPENDIX: FORCE CONSTANT EXPRESSIONS FOR THE TERSOFF POTENTIAL

The force constant matrix is defined by

$$D_{i\alpha j\beta}=\frac{\partial^2 U}{\partial r_{i\alpha}\partial r_{j\beta}}, \tag{A1}$$

where i and j denote the particle number, and α and $\beta=x$, y, and z.

First, consider the case when $i\neq j$,

$$\frac{\partial^2 U}{\partial r_{i\alpha}\partial r_{j\beta}}=\frac{\partial}{\partial r_{i\alpha}}\left(\sum_{l\neq j}\frac{\partial U}{\partial r_{jl}}\frac{\partial r_{jl}}{\partial r_{j\beta}}\right)=\frac{\partial}{\partial r_{i\alpha}}\left(\sum_{l\neq j}\frac{\partial U}{\partial r_{jl}}\frac{r_{jl\beta}}{r_{jl}}\right)=\sum_{l\neq j}\left[\frac{\partial^2 U}{\partial r_{i\alpha}\partial r_{jl}}\frac{r_{jl\beta}}{r_{jl}}+\frac{\partial U}{\partial r_{jl}}\frac{\partial}{\partial r_{i\alpha}}\left(\frac{r_{jl\beta}}{r_{jl}}\right)\right]=\frac{\partial U}{\partial r_{ij}}\frac{\partial}{\partial r_{i\alpha}}\left(\frac{r_{ji\beta}}{r_{ij}}\right)$$
$$+\sum_{l\neq j}\sum_{k\neq i}\frac{\partial^2 U}{\partial r_{ik}\partial r_{jl}}\frac{r_{ik\alpha}r_{jl\beta}}{r_{ik}r_{jl}}, \tag{A2}$$

where we have used the notation $r_{ji\beta}\equiv r_{j\beta}-r_{i\beta}$.

Using the fact that

$$\frac{\partial U}{\partial r_{ij}}=\frac{1}{2}\left(\frac{\partial V_{ij}}{\partial r_{ij}}+\frac{\partial V_{ji}}{\partial r_{ij}}\right)+\frac{1}{2}\sum_{k\neq i,j}\left(\frac{\partial V_{ik}}{\partial r_{ij}}+\frac{\partial V_{ki}}{\partial r_{ij}}+\frac{\partial V_{jk}}{\partial r_{ij}}+\frac{\partial V_{kj}}{\partial r_{ij}}\right), \tag{A3}$$

and

$$\sum_{l\neq j}\sum_{k\neq i}\frac{\partial^2 U}{\partial r_{ik}\partial r_{jl}}\frac{r_{ik\alpha}r_{jl\beta}}{r_{ik}r_{jl}}=\frac{1}{2}\sum_{l\neq j}\sum_{k\neq i}\frac{r_{ik\alpha}r_{jl\beta}}{r_{ik}r_{jl}}\left(\frac{\partial^2 V_{ik}}{\partial r_{ik}\partial r_{jl}}+\frac{\partial^2 V_{ki}}{\partial r_{ik}\partial r_{jl}}+\sum_{n\neq i,k}\frac{\partial^2 V_{in}}{\partial r_{ik}\partial r_{jl}}+\frac{\partial^2 V_{ni}}{\partial r_{ik}\partial r_{jl}}+\frac{\partial^2 V_{kn}}{\partial r_{ik}\partial r_{jl}}+\frac{\partial^2 V_{nk}}{\partial r_{ik}\partial r_{jl}}\right), \tag{A4}$$

Eq. (A2) becomes, after much algebraic manipulation, the following expression:

$$
\begin{aligned}
D_{i\alpha j\beta}=&\frac{1}{2}\left(\frac{r_{ij\alpha}r_{ij\beta}}{r_{ij}^3}-\frac{\delta_{\alpha\beta}}{r_{ij}}\right)\left(\frac{\partial V_{ij}}{\partial r_{ij}}+\frac{\partial V_{ji}}{\partial r_{ij}}\right)+\frac{1}{2}\frac{r_{ij\alpha}r_{ji\beta}}{r_{ij}^2}\left(\frac{\partial^2 V_{ij}}{\partial r_{ij}^2}+\frac{\partial^2 V_{ji}}{\partial r_{ij}^2}\right)+\frac{1}{2}\sum_{\substack{l\neq j\\ \mathrm{nn}(i)}}\left\{\left(\frac{r_{ij\alpha}r_{ij\beta}}{r_{ij}^3}-\frac{\delta_{\alpha\beta}}{r_{ij}}\right)\frac{\partial V_{il}}{\partial r_{ij}}+\frac{r_{ij\alpha}r_{ji\beta}}{r_{ij}^2}\frac{\partial^2 V_{il}}{\partial r_{ij}^2}\right.\\
&+\frac{r_{ij\alpha}r_{jl\beta}}{r_{ij}r_{jl}}\left(\frac{\partial^2 V_{ij}}{\partial r_{ij}\partial r_{jl}}+\frac{\partial^2 V_{il}}{\partial r_{ij}\partial r_{jl}}\right)+\frac{r_{il\alpha}r_{ji\beta}}{r_{il}r_{ij}}\left(\frac{\partial^2 V_{il}}{\partial r_{ij}\partial r_{il}}+\frac{\partial^2 V_{ij}}{\partial r_{ij}\partial r_{il}}\right)+\frac{r_{il\alpha}r_{jl\beta}}{r_{il}r_{jl}}\left(\frac{\partial^2 V_{il}}{\partial r_{il}\partial r_{jl}}+\frac{\partial^2 V_{ij}}{\partial r_{il}\partial r_{jl}}\right)\\
&\left.+\sum_{\substack{n\neq i,j,l\\ \mathrm{nn}(i)}}\left[\frac{r_{il\alpha}r_{ji\beta}}{r_{il}r_{ij}}\frac{\partial^2 V_{in}}{\partial r_{ij}\partial r_{il}}+\frac{r_{in\alpha}r_{jl\beta}}{r_{in}r_{jl}}\left(\frac{\partial^2 V_{ij}}{\partial r_{jl}\partial r_{in}}+\frac{\partial^2 V_{il}}{\partial r_{jl}\partial r_{in}}\right)\right]\right\}+\frac{1}{2}\sum_{\substack{l\neq i,j\\ \mathrm{nn}(j)}}\left\{\left(\frac{r_{ij\alpha}r_{ij\beta}}{r_{ij}^3}-\frac{\delta_{\alpha\beta}}{r_{ij}}\right)\frac{\partial V_{jl}}{\partial r_{ij}}+\frac{r_{ij\alpha}r_{jl\beta}}{r_{ij}r_{jl}}\left(\frac{\partial^2 V_{ji}}{\partial r_{ij}\partial r_{jl}}\right.\right.\\
&+\frac{\partial^2 V_{jl}}{\partial r_{ij}\partial r_{jl}}\Big)+\frac{r_{ij\alpha}r_{ji\beta}}{r_{ij}^2}\frac{\partial^2 V_{jl}}{\partial r_{ij}^2}+\frac{r_{il\alpha}r_{ji\beta}}{r_{il}r_{ij}}\left(\frac{\partial^2 V_{ji}}{\partial r_{ij}\partial r_{il}}+\frac{\partial^2 V_{jl}}{\partial r_{ij}\partial r_{il}}\right)+\frac{r_{il\alpha}r_{jl\beta}}{r_{il}r_{jl}}\left(\frac{\partial^2 V_{ji}}{\partial r_{il}\partial r_{jl}}+\frac{\partial^2 V_{jl}}{\partial r_{il}\partial r_{jl}}\right)\\
&\left.+\sum_{\substack{n\neq i,j,l\\ \mathrm{nn}(j)}}\left[\frac{r_{ij\alpha}r_{jl\beta}}{r_{ij}r_{jl}}\frac{\partial^2 V_{jn}}{\partial r_{ij}\partial r_{jl}}+\frac{r_{in\alpha}r_{jl\beta}}{r_{in}r_{jl}}\left(\frac{\partial^2 V_{ji}}{\partial r_{in}\partial r_{jl}}+\frac{\partial^2 V_{jn}}{\partial r_{in}\partial r_{jl}}\right)\right]\right\}+\frac{1}{2}\sum_{\substack{l\neq i,j\\ \mathrm{nn}(i)\\ \&\mathrm{nn}(j)}}\left\{\left(\frac{r_{ij\alpha}r_{ij\beta}}{r_{ij}^3}-\frac{\delta_{\alpha\beta}}{r_{ij}}\right)\left(\frac{\partial V_{li}}{\partial r_{ij}}+\frac{\partial V_{lj}}{\partial r_{ij}}\right)\right.\\
&+\frac{r_{il\alpha}r_{jl\beta}}{r_{il}r_{jl}}\left(\frac{\partial^2 V_{li}}{\partial r_{il}\partial r_{jl}}+\frac{\partial^2 V_{lj}}{\partial r_{il}\partial r_{jl}}\right)+\frac{r_{il\alpha}r_{ji\beta}}{r_{il}r_{ij}}\left(\frac{\partial^2 V_{li}}{\partial r_{il}\partial r_{ij}}+\frac{\partial^2 V_{lj}}{\partial r_{il}\partial r_{ij}}\right)+\frac{r_{ij\alpha}r_{jl\beta}}{r_{ij}r_{jl}}\left(\frac{\partial^2 V_{li}}{\partial r_{ij}\partial r_{jl}}+\frac{\partial^2 V_{lj}}{\partial r_{ij}\partial r_{jl}}\right)+\frac{r_{ij\alpha}r_{ji\beta}}{r_{ij}^2}\left(\frac{\partial^2 V_{li}}{r_{ij}^2}\right.\\
&+\frac{\partial^2 V_{lj}}{r_{ij}^2}\Big)+\sum_{\substack{n\neq i,j,l\\ \mathrm{nn}(l)}}\left[\frac{r_{in\alpha}r_{jl\beta}}{r_{in}r_{jl}}\left(\frac{\partial^2 V_{li}}{\partial r_{in}\partial r_{jl}}+\frac{\partial^2 V_{ln}}{\partial r_{in}\partial r_{jl}}\right)+\frac{r_{il\alpha}r_{jn\beta}}{r_{il}r_{jn}}\left(\frac{\partial^2 V_{lj}}{\partial r_{il}\partial r_{jn}}+\frac{\partial^2 V_{ln}}{\partial r_{il}\partial r_{jn}}\right)+\frac{r_{in\alpha}r_{ji\beta}}{r_{in}r_{ij}}\frac{\partial^2 V_{li}}{\partial r_{in}\partial r_{ij}}\right.\\
&\left.\left.+\frac{r_{il\alpha}r_{jl\beta}}{r_{il}r_{jl}}\frac{\partial^2 V_{ln}}{\partial r_{il}\partial r_{jl}}+\frac{r_{ij\alpha}r_{jn\beta}}{r_{ij}r_{jn}}\frac{\partial^2 V_{lj}}{\partial r_{ij}\partial r_{jn}}+\frac{r_{in\alpha}r_{jn\beta}}{r_{in}r_{jn}}\frac{\partial^2 V_{ln}}{\partial r_{in}\partial r_{jn}}\right]\right\},
\end{aligned}
\tag{A5}
$$

where $\mathrm{nn}(i)$ denotes the nearest neighbor of particle i.

Now let us consider the case when $i=j$,

$$
\begin{aligned}
\frac{\partial^2 U}{\partial r_{i\alpha}\partial r_{i\beta}}=&\frac{\partial}{\partial r_{i\alpha}}\left(\sum_{l\neq i}\frac{\partial U}{\partial r_{il}}\frac{r_{il\beta}}{r_{il}}\right)=\sum_{l\neq i}\frac{\partial U}{\partial r_{il}}\frac{\partial}{\partial r_{i\alpha}}\left(\frac{r_{il\beta}}{r_{il}}\right)+\sum_{l\neq i}\frac{r_{il\beta}}{r_{il}}\frac{\partial}{\partial r_{i\alpha}}\left(\frac{\partial U}{\partial r_{il}}\right)\\
=&\sum_{l\neq i}\frac{\partial U}{\partial r_{il}}\left(\frac{\delta_{\alpha\beta}}{r_{il}}-\frac{r_{il\alpha}r_{il\beta}}{r_{il}^3}\right)+\sum_{l\neq i}\sum_{k\neq i}\frac{r_{ik\alpha}r_{il\beta}}{r_{ik}r_{il}}\frac{\partial^2 U}{\partial r_{ik}\partial r_{il}}.
\end{aligned}
\tag{A6}
$$

This leads to the following expression for $D_{i\alpha i\beta}$:

$$
\begin{aligned}
D_{i\alpha i\beta}=&\frac{1}{2}\sum_{\substack{k\neq i\\ \mathrm{nn}(i)}}\left(\frac{r_{ik\alpha}r_{ik\beta}}{r_{ik}^2}\left(\frac{\partial^2 V_{ik}}{\partial r_{ik}^2}+\frac{\partial^2 V_{ki}}{\partial r_{ik}^2}\right)+\left(\frac{\delta_{\alpha\beta}}{r_{ik}}-\frac{r_{ik\alpha}r_{ik\beta}}{r_{ik}^3}\right)\left(\frac{\partial V_{ik}}{\partial r_{ik}}+\frac{\partial V_{ki}}{\partial r_{ik}}\right)+\sum_{\substack{l\neq i,k\\ \mathrm{nn}(i)}}\left\{\left(\frac{\delta_{\alpha\beta}}{r_{ik}}-\frac{r_{ik\alpha}r_{ik\beta}}{r_{ik}^3}\right)\frac{\partial V_{il}}{\partial r_{ik}}\right.\right.\\
&+\frac{r_{ik\alpha}r_{ik\beta}}{r_{ik}^2}\frac{\partial^2 V_{il}}{\partial r_{ik}^2}+\frac{r_{ik\alpha}r_{il\beta}}{r_{ik}r_{il}}\left[\frac{\partial^2 V_{il}}{\partial r_{ik}\partial r_{il}}+\frac{\partial^2 V_{ik}}{\partial r_{ik}\partial r_{il}}+\sum_{\substack{n\neq i,k,l\\ \mathrm{nn}(i)}}\left(\frac{\partial^2 V_{in}}{\partial r_{ik}\partial r_{il}}\right)\right]\Big\}+\sum_{\substack{l\neq i,k\\ \mathrm{nn}(k)}}\left[\left(\frac{\delta_{\alpha\beta}}{r_{ik}}-\frac{r_{ik\alpha}r_{ik\beta}}{r_{ik}^3}\right)\frac{\partial V_{kl}}{\partial r_{ik}}+\left(\frac{\delta_{\alpha\beta}}{r_{ik}}\right.\right.\\
&\left.-\frac{r_{ik\alpha}r_{ik\beta}}{r_{ik}^3}\right)\left(\frac{\partial V_{ki}}{\partial r_{il}}+\frac{\partial V_{kl}}{\partial r_{il}}\right)+\left(\frac{r_{il\alpha}r_{ik\beta}}{r_{il}r_{ik}}+\frac{r_{ik\alpha}r_{il\beta}}{r_{il}r_{ik}}\right)\left(\frac{\partial^2 V_{ki}}{\partial r_{ik}\partial r_{il}}+\frac{\partial^2 V_{kl}}{\partial r_{ik}\partial r_{il}}\right)+\frac{r_{ik\alpha}r_{ik\beta}}{r_{ik}^2}\frac{\partial^2 V_{kl}}{\partial r_{ik}^2}+\frac{r_{il\alpha}r_{il\beta}}{r_{il}^2}\left(\frac{\partial^2 V_{ki}}{\partial r_{il}^2}+\frac{\partial^2 V_{kl}}{\partial r_{il}^2}\right)\\
&\left.\left.+\sum_{\substack{n\neq i,k,l\\ \mathrm{nn}(k)}}\left(\frac{r_{il\alpha}r_{in\beta}}{r_{il}r_{in}}\frac{\partial^2 V_{ki}}{\partial r_{in}\partial r_{il}}\right)\right]\right).
\end{aligned}
\tag{A7}
$$

Expressions for the above derivatives in terms of the parameters of the Tersoff potential can be found in Appendix B of Ref. 33. A computer code was written to implement Eqs. (A5) and (A7), and the diagonalization of the resulting matrix yields the phonon frequencies utilized in the main text.

[1] J. Justo, V. Bulatov, and S. Yip, Scrip. Met. (in press).
[2] L. Porter, J. Li, and S. Yip (unpublished); J. Li, L. Porter, and S. Yip, J. Nucl. Mater. (submitted for publication).
[3] O. Sugino and R. Car, Phys. Rev. Lett. **74**, 1823 (1995).
[4] V. V. Bulatov, S. Yip, A. S. Argon, Philos. Mag. **72**, 453 (1995); T. A. Arias, V. V. Bulatov, S. Yip, and A. S. Argon, (unpublished).
[5] M. Tang and S. Yip, Phys. Rev. Lett. **75**, 2738 (1995).
[6] F. Stillinger and T. Weber, Phys. Rev. B **31**, 5262 (1985).
[7] J. Tersoff, Phys. Lett. **56**, 632 (1986).
[8] J. Tersoff, Phys. Rev. B **37**, 6991 (1988).
[9] J. Tersoff, Phys. Rev. B **38**, 9902 (1988).
[10] B. W. Dodson, Phys. Rev. B **35**, 2795 (1987).
[11] K. E. Khor and S. Das Sarma, Phys. Rev. B **38**, 3318 (1988).
[12] J. R. Chelikowsky, J. C. Phillips, M. Kamal, and M. Strauss, Phys. Rev. Lett. **62**, 292 (1989).
[13] G. C. Abell, Phys. Rev. B **31**, 6184 (1985).
[14] A. P. Horsfield, A. M. Bratkovsky, M. Fearn, D. G. Pettifor, and M. Aoki, Phys. Rev. B **53**, 12 694 (1996).
[15] M. Tang and S. Yip, Phys. Rev. B **52**, 1 (1995).
[16] M. Parrinello and A. Rahman, J. Appl. Phys. **52**, 7182 (1981).
[17] C. Z. Wang, C. T. Chan, and K. M. Ho, Phys. Rev. B **42**, 276 (1990).
[18] J. Q. Broughton and X. P. Li, Phys. Rev. B **35**, 9120 (1987).
[19] S. J. Cook and P. Clancy, Phys. Rev. B **47**, 7686 (1993).
[20] M. Ishimaru, K. Yoshida, and T. Motooka, Phys. Rev. B **53**, 7176 (1996).
[21] P. J. Ungar, T. Halicioglu, and W. A. Tiller, Phys. Rev. B **50**, 7344 (1994).
[22] R. Najafabadi and D. J. Srolovitz, Phys. Rev. B **52**, 9229 (1995).
[23] J. F. Lutsko, D. Wolf, S. R. Phillpot, and S. Yip, Phys. Rev. B **40**, 2841 (1989).
[24] *Landolt-Börnstein* (Springer, Berlin, 1982), Vol. 17.
[25] I. Barin and O. Knake, *Thermochemical Properties of Inorganic Substances* (Springer, Berlin, 1973).
[26] P. Flubacher, A. J. Leadbetter, and J. A. Morrison, Philos. Mag. **4**, 273 (1959).
[27] N. W. Ashcroft and N. D. Mermin, *Solid State Physics* (Saunders College, Philadelphia, 1976), Chap. 25.
[28] B. A. Weinstein and G. J. Piermarini, Phys. Rev. B **12**, 1172 (1975).
[29] S. Wei, C. Li, and M. Y. Chou, Phys. Rev. B **50**, 14 587 (1994).
[30] C. H. Xu, C. Z. Wang, C. T. Chan, and K. M. Ho, Phys. Rev. B **43**, 5024 (1991).
[31] J. Tersoff, Phys. Rev. B **39**, 5566 (1989).
[32] L. Porter (unpublished).
[33] M. Tang, Ph.D. thesis, Massachusetts Institute of Technology, Department of Nuclear Engineering, 1995.